Anisotropy Enhanced Phase Separation in Polymer Dispersed Liquid Crystals

Farida Benmouna[*] and Mustapha Benmouna

Faculty of Sciences, University of Tlemcen, BP 119, 13000, Algeria

Abstract: Phase separated blends of polymers and low molecular weight liquid crystals, commonly known as polymer dispersed liquid crystals in short PDLCs, are investigated. These materials offer a realm of applications in modern technologies, including sensors, commutable windows, display devices and telecommunication systems. A particular attention is given to the effects of anisotropy of the liquid crystal on the phase behavior under equilibrium and non equilibrium conditions. The theoretical formalism used is based on the lattice model of isotropic mixing, combined with standards theories of nematic and smectic-A orders. Considering the equilibrium phase behavior, we find that the nematic order enhances the polymer / solvent phase separation, and that the osmotic pressure shows substantial changes for relatively small polymer volume fractions. We find that the anisotropy enhanced phase separation is more pronounced for a smectic-A liquid crystal, and the miscibility gap is widened. The kinetics of swelling by nematic LCs is examined using a linear solvent diffusion process, with a rate of swelling directly related to the derivative of the osmotic pressure. An abrupt swelling / de-swelling transition is found, due to overwhelming effects of the anisotropic interaction beyond the threshold LC concentration. Anisotropy enhanced phase separation is also investigated in the method of synthesis based on the polymerization induced phase separation mechanism. We find that the kinetics of separation during early stages of polymerization is faster, due to the anisotropic interaction of the low molecular weight solvent. The kinetics speed up is favored by the long range viscous flow effects due to hydrodynamic interactions. A limited selection of experimental data in the literature is chosen to validate some theoretical predictions obtained from the present formalisms.

Keywords: PDLCs, anisotropy, nematic, phase separation, swelling, kinetics, PIPS.

INTRODUCTION

Polymer dispersed liquid crystals (PDLCs) form a special class of composite materials made of a polymer matrix containing pores filled with a low molecular weight liquid crystal (LC), and as such, they are said to have a Swiss cheese morphology [1, 2]. PDLCs have drawn a particular attention in the literature from both fundamental and applied points of view, for their importance in a realm of modern technologies, and interesting properties encompassing morphology, structure, thermodynamic, thermo mechanical and viscoelastic aspects [3-10]. They offer major advantages over materials with similar functionalities because of their high availability, and competitive costs. A large choice of monomers is offered for the preparation of PDLCs either from natural or synthetic origin. LCs can be used as individual species or hooked to the polymer backbone directly via covalent bounds, or indirectly through flexible spacers with controlled length [11]. The synthesis is rather simple and relies on standard equipments. Essentially, three methods of preparation are adopted known as Solvent Induced Phase Separation (SIPS), Thermally Induced Phase Separation (TIPS) and Polymerization Induced Phase Separation (PIPS) [12]. A common feature of these methods is the fact that polymer and LC phase separate to yield a polymer matrix hosting a pure LC phase confined in droplets. The latter governs the main features of the functionalities desired for the composite material and the requirements for each application. In the SIPS process, polymer and LC are mixed with solvent and emulsifier to get an initial homogenous solution. Then, solvent is evaporated at a certain rate, inducing phase separation and subsequent formation of LC droplets in the Swiss cheese format indicated above. The TIPS procedure consists of heating the polymer / LC solution above the critical temperature T_C (for a system exhibiting Upper Critical Solution Temperature), where a homogenous monophase state is reached. A sudden quench into the biphasic region is executed, and after a certain period of time, depending on thermodynamic and hydrodynamic properties of the medium, the system reaches an equilibrium state with two coexisting phases. In the PIPS process, a photo polymerization is used to transform the initial monomer / LC solution into a solid product, which comes out of a subtle competition between the kinetics of polymerization and phase separation [13]. This process will be examined in details later in this work.

The interest on PDLCs originates from their broad spectrum of applications in modern technologies, ranging from switchable windows with controlled light transmission, display panels, telecommunication systems, and high performance optical switches and

*Address correspondence to this author at the Faculty of Sciences, University of Tlemcen, BP 119, 13000, Algeria; Tel: +213 7 75 15 11 75;
E-mail: fbenmouna@email.com

sensing devices. Their responsiveness to external excitations, using electric or magnetic fields makes them good candidates for developing new functionalities in smart materials. Photonic and opto-electronic devices are being continuously improved by a better control of the properties of anisotropy related with optical and dielectric functions [14]. The interplay between flexibility and rigidity of liquid crystalline polymers, combined with their electrical responsiveness to pressure variations suggests their use as artificial muscle implants [15].

This paper is organized as follows: the following section gives the theoretical formalism needed to construct the phase diagram under a variety of conditions, with a particular attention given to the effects of anisotropy encompassing nematic, smectic-A and nematogen mixtures. The thermodynamic properties that govern the isotropic mixing of molecular species are specified. Then, the focus will be more on the considerations of the anisotropy enhanced phase separation. A variety of examples are presented to highlight the effects of anisotropy on equilibrium and non equilibrium properties. Widening of phase separated regions due to the anisotropy is discussed, considering examples of equilibrium phase diagrams for monomer solutions and polymer / LC blends. The kinetics of swelling in the presence of LC and the effects of anisotropy on the polymerization induced phase separation are discussed in this section using simplified models.

Examples to confront the theoretical predictions with the experimental observations are given before prospects for the future and the conclusions.

THEORETICAL FORMALISM

Free Energy and Chemical Potentials of Isotropic Mixing

In the lattice model [16], the free energy density for isotropic mixing of blend A/B can be written as

$$\frac{f^{(i)}}{k_B T} = \frac{\varphi_a}{N_a}\ln\varphi_a + \frac{\varphi_b}{N_b}\ln\varphi_b + \chi\varphi_a\varphi_b \qquad (1)$$

Here, superscript (i) stands for isotropic, N's and φ's represent the degree of polymerisation and volume fraction of the molecular species indicated by the subscript letter, respectively, χ_{ab} is the interaction parameter between A and B monomers, k_B the Boltzmann's constant and T the absolute temperature.

The total free energy of the blend is $F = N_T f$ where N_T is the total number of lattice sites. B-species represents the low molecular weight liquid crystal (LC with $N_b \cong 1$), while A is the linear polymer. For crosslinked networks, one should add the rubber elasticity contribution that opposes polymer stretching. This case is well documented in the literature and will not be considered because; we focus more on the anisotropy effects coming from the LC component.

In the isotropic limit, the phase behaviour is controlled by the parameter χ_{ab} which is mainly temperature dependent. Note that the chemical potentials of A and B are defined as [17, 18]

$$\mu_a = \frac{\partial F}{\partial n_a}\bigg)_{T,n_b}; \qquad \mu_b = \frac{\partial F}{\partial n_b}\bigg)_{T,n_a}. \qquad (2)$$

The composition of coexisting phases (with and without primes) are determined by solving simultaneously the set of equations

$$\mu_a = \mu_a'; \qquad \mu_b = \mu_b'. \qquad (3)$$

The region where coexisting phases are in equilibrium is delimited by the spinodal equation

$$\frac{\partial^2 f}{\partial \varphi_b^2} = 0. \qquad (4)$$

The explicit forms of the isotropic chemical potentials are obtained as

$$\mu_a^{(i)} = \ln\varphi_a + \left(1 - \frac{N_a}{N_b}\right)\varphi_b + \chi_{ab}N_a\varphi_b^2 \qquad (5)$$

$$\mu_b^{(i)} = \ln\varphi_b + \left(1 - \frac{N_b}{N_a}\right)\varphi_a + \chi_{ab}N_b\varphi_a^2, \qquad (6)$$

While the critical parameter $\chi_s^{(i)}$ for spinodal decomposition is expressed in terms of φ's and N's as follows

$$\chi_s^{(i)} = \frac{1}{2}\left[\frac{1}{N_a\varphi_a} + \frac{1}{N_b\varphi_b}\right]. \qquad (7)$$

The number of units in the LC N_b appears explicitly here, but in the numerical computations it is left to be one.

Anisotropic Free Energy, Chemical Potentials and Order Parameters

Under the conditions where the solvent molecules exhibit a nematic order, the free energy density must be written as the sum of isotropic and anisotropic contributions. The latter is obtained using standard theories as [19]

$$\frac{f^{(a)}}{k_B T} = \varphi_b \left[-\ln Z + \frac{1}{2} v \varphi_b s^2 \right] \tag{8}$$

Where s is the nematic order parameter

$$s = \frac{1}{2} \left[3 \left\langle \cos^2 \theta \right\rangle - 1 \right] \tag{9}$$

The symbol $\left\langle \ \right\rangle$ designates an average with respect to the θ-angle distribution function $\psi(\theta)$

$$\psi(\theta) = Z^{-1} \exp - \left[\frac{U(\theta)}{k_B T} \right] \tag{10}$$

$U(\theta)$ is the nematic interaction potential, and Z the partition function

$$\frac{U(\theta)}{k_B T} = -\frac{m_n}{2} \left[3 \left\langle \cos^2 \theta \right\rangle - 1 \right];$$

$$Z = 2\pi \int_0^\pi d\theta \exp - \left[\frac{U(\theta)}{k_B T} \right] \sin \theta. \tag{11}$$

In the mean field approximation, the nematic potential has an amplitude $m_n = v\varphi_b s$, and the quadrupole parameter v is function of the ratio T/T_{NI}, T_{NI} being the nematic to isotropic transition temperature

$$v = 4.54 \frac{T_{NI}}{T} \tag{12}$$

A first order transition between isotropic and nematic phase occurs when both the free energy and its derivative with respect to s are equal to zero. Solving the resulting equations for $\varphi_b = 1$ yields, $s = 0$ for the isotropic phase, and 0.429 for the nematic one, leading to $v_{NI} = 4.54$ as illustrated in Figure **1a** on the left hand side (LHS) for a pure LC ($\varphi_b = 1$), while panel b corresponds to the case where $\varphi_b = 0.9$.

The order parameter can be calculated from the partition function by using

$$s = \frac{\partial}{\partial m_n} \ln Z. \tag{13}$$

Figure **2** shows the variations of s with T and φ_b. Upon cooling down, the LC concentration at which the nematic order becomes effective drops significantly. Above T_{NI}, the system exhibits a nematic order in a tiny range of φ_b, close to 1. The plots in Figure **2a** are grouped in panel **b** as a single master curve representing s versus φ_b/φ_{NI}.

For a LC exhibiting a smectic-A order, the extended theories [19] can be used including a new order parameter denoted σ

$$\sigma = \frac{1}{2} \left\langle \left(3\cos^2 \theta - 1 \right) \cos 2\pi \frac{z}{d} \right\rangle, \tag{14}$$
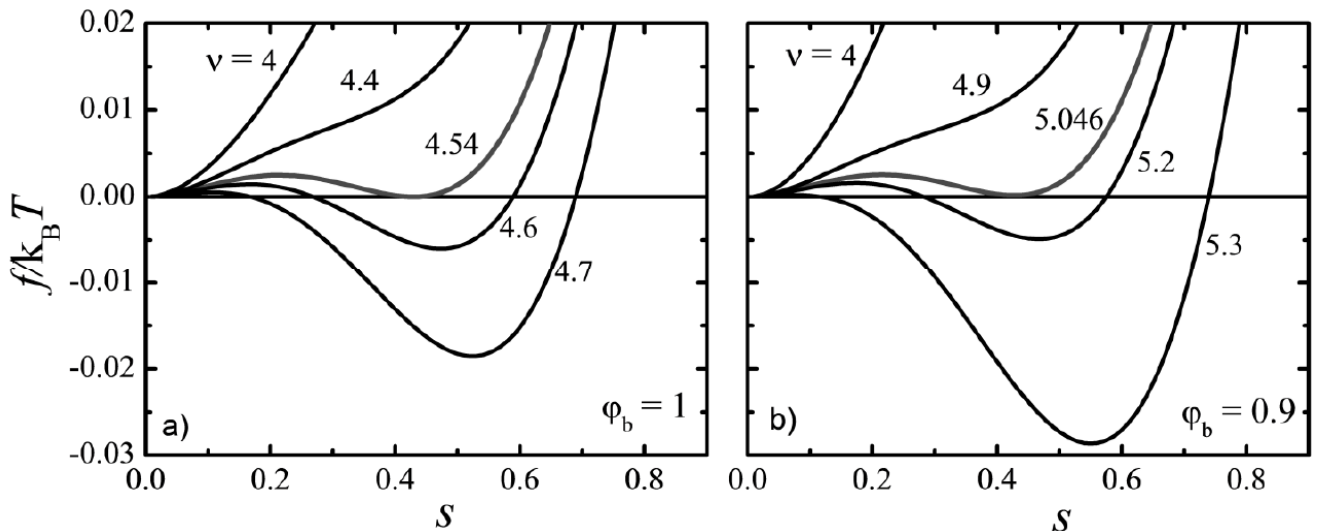
Figure 1: $f/k_B T$ vs s. **a)** Pure LC, $\varphi_b = 1$, the curve with $v = 4.54$ explains the factor in front of Eq. (12). **b)** $\varphi_b = 0.9$.
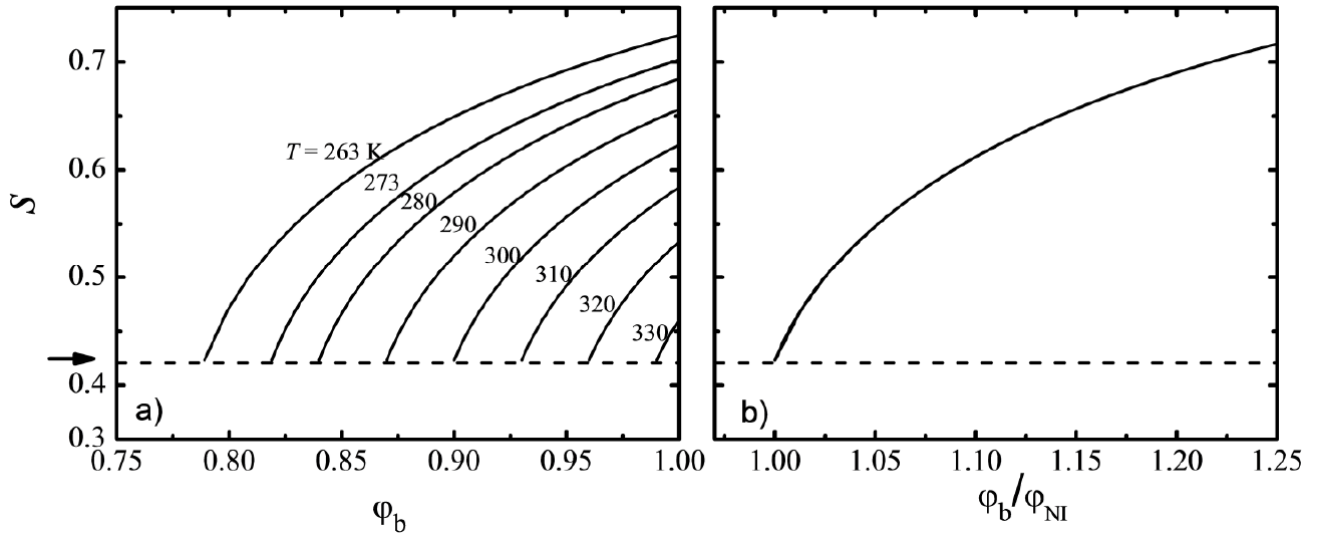
Figure 2: a) s vs φ_b of the eutectic mixture E7 with T_{NI} = 333 K. The arrow indicates s_c = 0.429. **b**) The master curve giving s vs φ_b/φ_{NI}.

Hence, the anisotropic free energy density becomes

$$\frac{f^{(a)}}{k_B T} = \varphi_b \left[-\ln Z + \frac{1}{2} v \varphi_b \left(s^2 + \alpha \sigma^2 \right) \right], \tag{15}$$

While the partition function Z combines integrations over $\mu = \cos\theta$ and z

$$Z = 2\pi \int_0^1 d\mu \int_0^d \exp\left[\frac{m_n}{2} \left(3\mu^2 - 1 \right) \frac{m_s}{2} \left(3\mu^2 - 1 \right) \cos 2\pi \frac{z}{d} \right] dz. \tag{16}$$

There are two mean field parameters m_n and m_s, functions of s and σ according to

$$m_n = v \varphi_b s \qquad m_s = \alpha v \varphi_b \sigma. \tag{17}$$

The constant α depends on T_{NI} and T_{SN}, where T_{SN} represents the smectic to nematic transition temperature. The order parameters s and σ are calculated in terms of T and φ_b by solving self consistently Eqs. (13) to (17). In order to ease the numerical calculations, we write the partition function in terms of the zero order modified Bessel function $I_0(u)$

$$Z = \int_0^\pi d\mu \exp\left[\frac{m_n}{2} \left(3\mu^2 - 1 \right) \right] I_0 \left(\frac{m_s}{2} \left(3\mu^2 - 1 \right) \right), \tag{18}$$

$$I_0(u) = \frac{1}{\pi} \int_0^\pi \exp\left[u \cos\psi \right] d\Psi,$$

Under the present conditions, the argument of the Bessel function in Eq. (18) does not exceed 3.5, which means that $I_0(u)$ can be approximated with
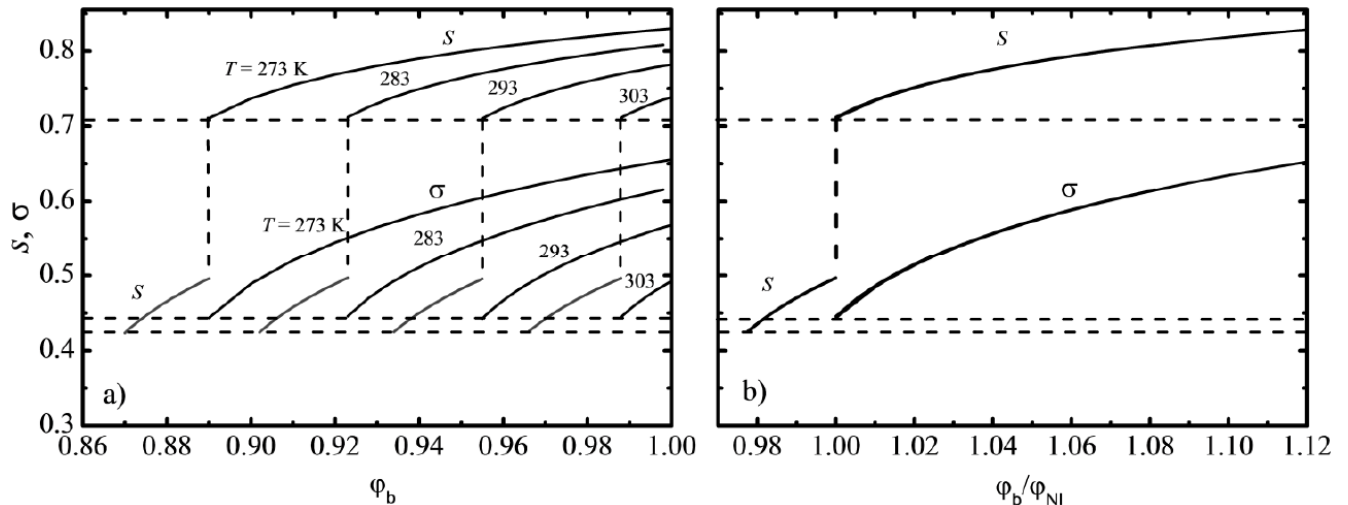
Figure 3: a) s and σ vs φ_b and T separately. **b**) s and σ vs φ_b/φ_{NI}. (8CB, T_{SN} = 306.5 K, T_{NI} = 313.5 K and α = 0.9375).

$$I_0(u) \approx 1 + 3.5156u^2 + 3.08999429u^4 + 1.2067492u^6 + \tag{19}$$
$$0.2659732u^8 + 0.0360768u^{10} + 0.0045813u^{12}$$

As a particular example, we consider the LC 8CB characterized by T_{SN} = 33.5°C, T_{NI} = 40.5°C, yielding successive transitions from smectic to nematic to isotropic phases. These transitions are illustrated in Figure **3** where the variations of s and σ versus T and φ_b are shown. Both increase monotonically with φ_b, but s undergoes a discontinuous jump upward at $\varphi_b = \varphi_{SN}$, signalling a first order transition. In part b, we show how the order parameters vary with the lumped variable φ_b/φ_{NI}.

According to this theory, one has α = 0.98 if $T_{SN} = T_{NI}$ and the LC exhibits a direct transition from smectic-A to isotropic state. But if $T_{SN} < T_{NI}$, then $\alpha < 0.98$ and the LC undergoes successive transitions S → N → I. Note that σ drops abruptly to 0 when φ_b reaches the limit $\varphi_{SN} = T_{SN}/T_{NI}$, and the LC undergoes a first order transition S → N. The nematic order persists for $T_{NI} < T < T_{SN}$, but the LC becomes isotropic at $T \geq T_{NI}$. Figure **4** represents the case of a hypothetic LC with $T_{SN} = T_{NI}$ = 333 K, and characterized by a first order transition from smectic-A to isotropic phase.

To complete the phase diagram, one needs the anisotropic chemical potentials and spinodal equation defined by the second derivative of the free energy. Those are given below as

$$\mu_a^{(a)} = \frac{1}{2}\frac{N_a}{N_b}\left[s^2 + \alpha\sigma^2\right]\nu\varphi_b^2, \tag{20}$$

$$\mu_b^{(a)} = -\ln Z + \frac{1}{2}\left[s^2 + \alpha\sigma^2\right]\nu\varphi_a^2, \tag{21}$$

$$\frac{\partial^2 f^{(a)}}{\partial\varphi_b^2} = \frac{\nu s}{N_b}\left(s + \varphi_b\frac{\partial s}{\partial\varphi_b}\right) - \frac{\nu\alpha\sigma}{N_b}\left(\sigma + \varphi_b\frac{\partial\sigma}{\partial\varphi_b}\right). \tag{22}$$

The equilibrium phase diagrams were reported in [17-19] under a variety of conditions, and will not be reproduced here.

Another class of PDLCs can be considered when the polymer backbone itself carries nematic LC groups. Here, one deals with a nematogen mixture whereby a coupling takes place between the free LC molecules and the side groups, giving rise to a rich variety of phases. For a weak coupling, two distinct nematic phases are obtained reflecting the properties of each component. Interestingly, a single nematic phase emerges for a strong coupling. For such mixtures, one has two transition temperatures (T_{N1a}, T_{N1b}) and three quadrupole parameters ν_{ij} given by

$$\nu_{aa} = 4.54\frac{T_{N1a}}{T}; \quad \nu_{bb} = 4.54\frac{T_{N1b}}{T}; \quad \nu_{ab} = \beta\sqrt{\nu_{aa}\nu_{bb}}. \tag{23}$$

The strength of coupling is determined by the factor β in ν_{ab}; which is higher or lower than 1 depending on the degree of coupling between the two nematogens. It is important to keep in mind that binding the LC groups to the polymer backbone can modify substantially its transition temperatures compared to those of the free LC. The anisotropic free energy density for the mixture is
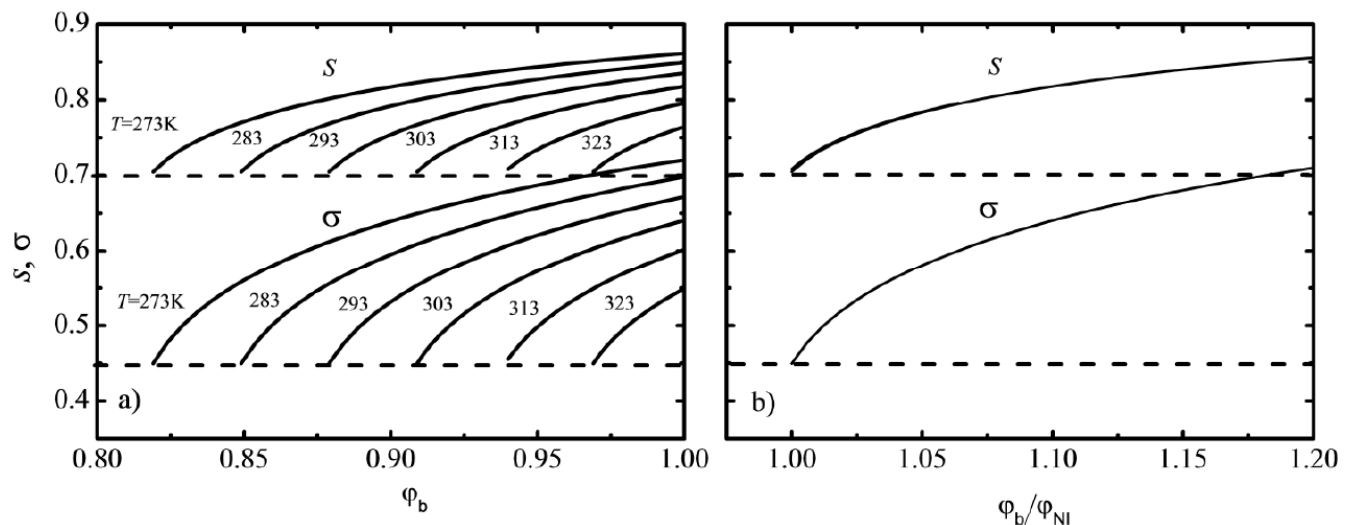
Figure 4: a) s and σ vs φ_b and T **b**) s and σ vs φ_b/φ_{NI}. To plot these curves, we used $T_{SN} = T_{NI}$ = 333 K and α = 0.98.

$$\frac{f^{(n)}}{k_B T} = -\varphi_a \ln Z_a - \varphi_b \ln Z_b +$$

$$\frac{1}{2}\left(\nu_{aa}\varphi_a^2 s_a^2 + \nu_{bb}\varphi_b^2 s_b^2 + 2\nu_{ab}\varphi_a\varphi_b s_a s_b\right). \qquad (24)$$

The partition functions and order parameters are

$$Z_i = 2\pi \int_0^1 d\mu \exp\left[\frac{m_i}{2}\left(3\mu^2 - 1\right)\right]; \qquad (25)$$

$$s_i = \frac{\partial}{\partial m_i}\ln Z_i \quad (i = a,b).$$

Minimizing the free energy with respect to s_a and s_b yields the mean field parameters m_a and m_b as

$$\begin{pmatrix} m_a \\ m_b \end{pmatrix} = \begin{pmatrix} \nu_{aa} & \nu_{ab} \\ \nu_{ab} & \nu_{bb} \end{pmatrix}\begin{pmatrix} \varphi_a s_a \\ \varphi_b s_b \end{pmatrix}. \qquad (26)$$

As a particular example, we choose the weak coupling limit and compute s_a and s_b for T_{NIa} = 333 K, T_{NIb} = 343 K and β = 0.8. Figure **5** shows that both order parameters decrease in the lower range of φ_b, go through a minimum before increasing as φ_b approaches one. There are two separate branches near T_{NI}. The calculations for β = 1 (intermediate coupling) show that the curves are monotonically decreasing, and for β > 1 (strong coupling), s_a and s_b increase with φ_b, admit a maximum before decreasing.

The phase diagrams of nematogen mixtures are quite rich exhibiting features of the polymer for small φ_b and those of the free LC in the vicinity of φ_b = 1. In between, there is a variety of regions with phase properties depending on the strength of coupling [20].
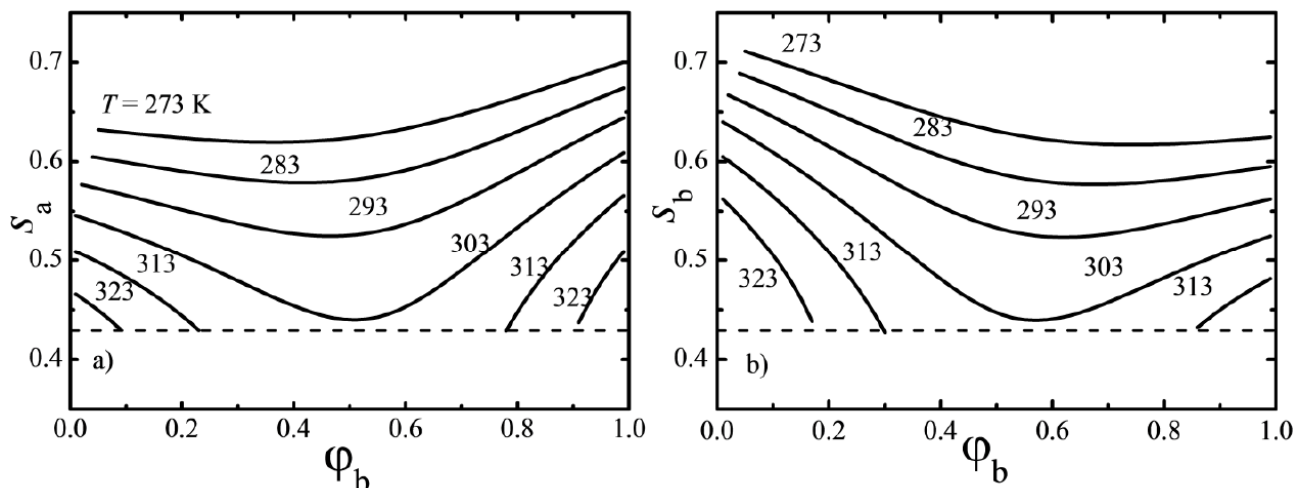
Anisotropy Enhanced Phase Separation

We first recall that in the case of isotropic solvents, the phase behaviour is governed by the parameter χ_{ab} expressing short range excluded volume interactions. In dilute solutions, for χ_{ab} > ½, polymer chains experience poor solvent conditions, and contract leading to a phase separation from the solvent. This transition process is remarkably enhanced in the case of anisotropic solvents. We will scrutinize this enhancement below by considering equilibrium and non equilibrium properties.

Equilibrium Phase Behaviour

The anisotropy enhanced phase separation for nematic LCs can be visualized by considering the chemical potential μ_b or, equivalently the osmotic pressure $\pi = -v_0\mu_b$, where the solvent molar volume v_0 is constant. This potential is the sum of isotropic (Eq. 6) and anisotropic (Eq. 21) contributions. For nematic LCs, we only need to put $\sigma = 0$ in Eq. 21. Under good solvent conditions, the polymer favours contact with solvent and swells, but as the miscibility drops, the solvent is rejected by polymer inducing deswelling.

Figure **6a** illustrates the nematic enhanced deswelling of the polymer. Under good solvent conditions (T = 360 K > T_C), π decreases steadily with φ_a^{-1} but for poor solvents (T = 295 K < T_C), the curve π vs φ_a^{-1} undergoes a discontinuous transition and the system exhibits two coexisting phases with different compositions. The anisotropy introduces important changes in the range of small φ_a. It favours phase separation as long as the nematic order parameter exceeds the threshold and $\varphi_b > \varphi_{NI}$. Panel b of Figure **6** gives the phase diagram including the binodal (solid)

Figure 5: a) s_a and **b)** s_b vs φ_b and T. To plot these curves, we used T_{NIa} = 333 K, T_{NIb} = 343 K and β = 0.8.
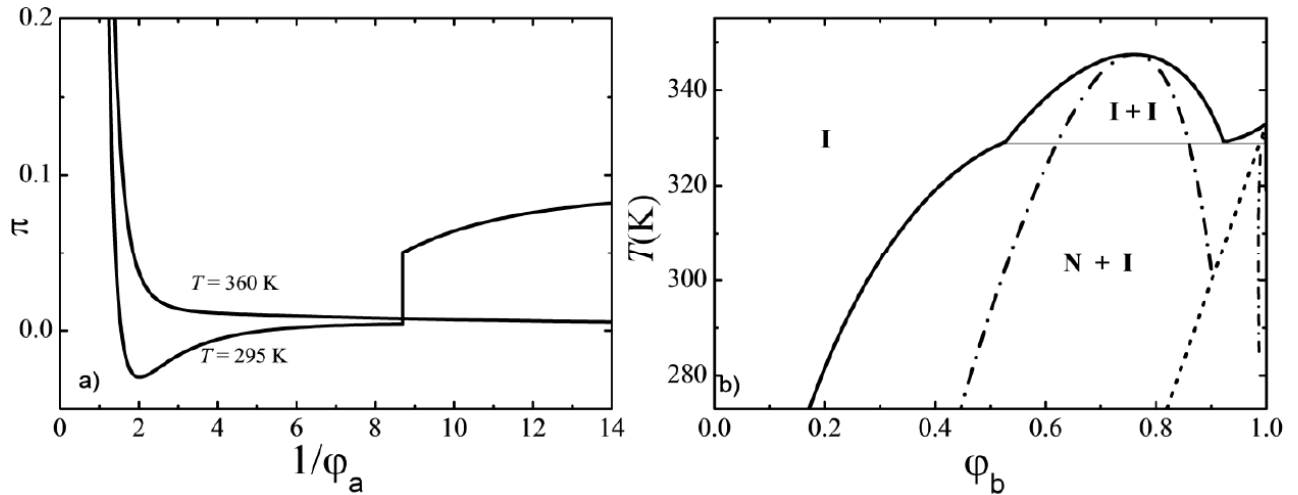
Figure 6: a) Osmotic pressure π vs $1/\varphi_a$ at *T*= 295 K and *T*= 360 K. **b**) Phase diagram *T* vs φ_b, solid line represents the binodal and dashed lines represent the spinodal. The parameters used are χ_{ab} = −0.4 + 440/*T*, N_a = 10, N_b = 1, T_C = 347.49 K, T_{NI} = 313.5 K. The letters N and I stand for nematic and isotropic, respectively.

and the spinodal (dashed) curves. It is significantly distorted by the anisotropy for $\varphi_b > \varphi_{NI}$, where biphasic regions are widened as the system is cooled down, and φ_b increases further above φ_{NI}.

The anisotropy driven phase separation is more pronounced for a LC with a higher degree of order. For example, in the case of a smectic-A LC such as 8CB, tendencies towards phase separation are enhanced as illustrated in the free energy plots of Figure **7**. Panel a shows the case of a nematic LC such as 5CB (T_{NI} = 313.5 K), while panel b corresponds to the smectic LC, 8CB. One clearly sees that the biphasic region delimited by the free energy curve and the double tangent is wider for 8CB.

The enhanced anisotropy driven phase separation for a higher order LC is confirmed in Figures **8a** and **8b**, where the diagrams for the initial monomer solution and the final blends are given.

Kinetics of Swelling

The kinetics of polymer swelling was a subject of a particular attention for decades, because of its relevance to a variety of applications based on linear polymers (coil globule transition) or crosslinked networks (swelling / deswelling of gels). Starting from the general kinetic equation for the time evolution of $\varphi_a(t)$

$$\frac{\partial \varphi_a(t)}{\partial t} = F\left(\left[\varphi_a(t)\right]\right) + g(t). \tag{27}$$

Were, in general, $F(\varphi_a)$ is a non linear functional of $\varphi_a(t)$, g(t) is a noise that generates random fluctuations
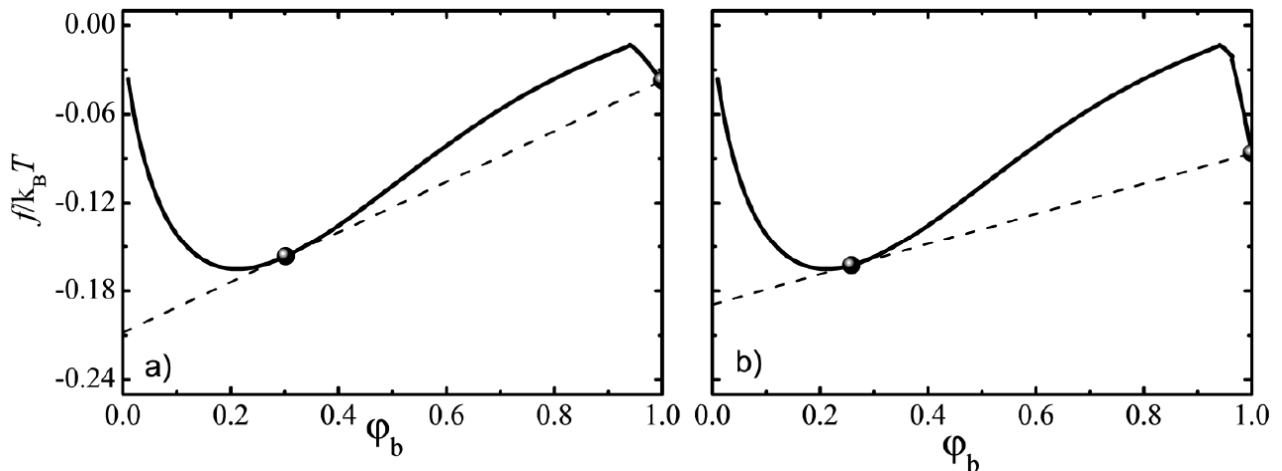
Figure 7: $f/k_B T$ vs φ_b **a**) Polymer / 5CB with T_{NI} = 313.5 K. **b**) Polymer / 8CB with T_{SN} = 306.5 K, T_{NI} = 313.5 K. To plot these curves, we used *T* = 295 K, N_a=10, N_b = 1, and α = 0.9375, χ = −0.4+440/*T*. Filled circles mark the tangent points.
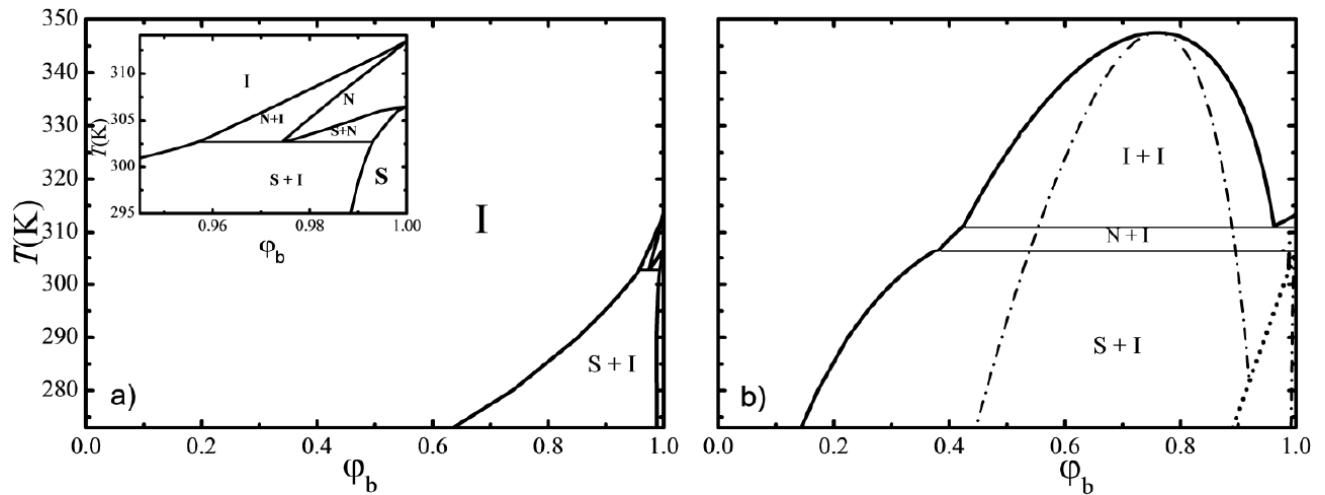
Figure 8: Phase diagram T vs φ_b for **a**) Monomer / 8CB with $N_a = 1$, $T_C = 183.33$ K. Insert is an enlarged view near $\varphi_b = 1$. **b**) Polymer / 8CB with $N_a = 10$, $T_C = 347.49$ K. Continuous lines represent the binodals, dashed lines are spinodal curves. The parameters used for these plots are $\chi = -0.4 + 440/T$, $T_{SN} = 306.5$ K, $T_{NI} = 313.5$ K. I = isotropic, N = nematic, S = smectic.

of $\varphi_a(t)$ from its mean. A linearization of the functional $F(\varphi_a)$, supplemented with the use of standard statistical properties of the noise, lead to a linear kinetic equation for the mean. Assuming that initially, the polymer is dry, but after complete swelling, its volume fraction reaches $\varphi_{a\infty}$, the swelling kinetics is found to satisfy a simple exponential form as

$$\frac{\varphi_a(t) - \varphi_{a\infty}}{\varphi_{a0} - \varphi_{a\infty}} = e^{-t/\tau_{SW}}, \tag{28}$$

The characteristic time of swelling τ_{sw} depends on the osmotic pressure π, the monomer diffusion coefficient $D_m = k_B T/6\pi\eta_0 l$ (η_0 being the solvent viscosity, and l the monomer length), and the chain radius of gyration R_g

$$\tau_{sw} = \frac{D_m}{R_g^2 \, \partial\pi/\partial\varphi_a}. \tag{29}$$

Combining Eqs. (6,7) and (21,22) for the nematic LC, yields

$$\tau_{sw}^{-1} = \tau_0^{-1} \left\{ \frac{1}{N_a\varphi_a} + \frac{1}{N_b\varphi_b} - 2\chi_{ab} - \frac{\nu s}{N_b}\left(s + \varphi_b \frac{\partial s}{\partial\varphi_b}\right)\right\}, \tag{30}$$

Note that the quantity $\tau_0 = R_g^2/D_m$ represents the time over which the chain diffuses a distance equivalent to its radius of gyration. The ratio τ_0/τ_{sw} is plotted as a function of φ_b in Figure **9,** to highlight the effects of anisotropy on the kinetics of swelling. One notes that, as long as the isotropic interaction due to the interaction χ_{ab} dominates, the polymer swelling
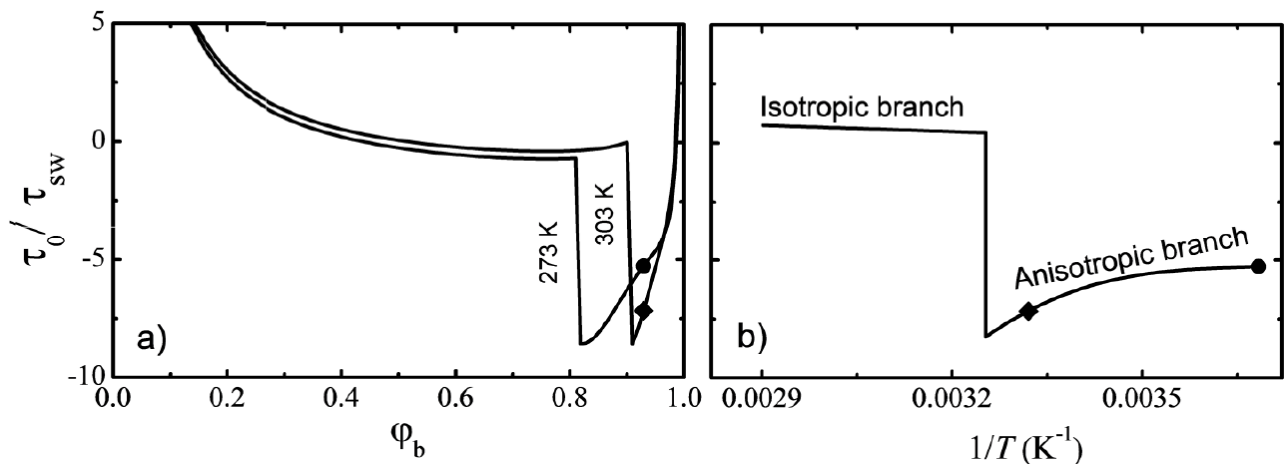
Figure 9: a) τ/τ_{sw} vs φ_b at $T = 273$ and 303 K. For $\varphi < \varphi_{NI}$, the isotropic branch does not change much with T while the nematic branch shifts to the right upon heating b) τ_0/τ_{sw} vs T^{-1} at $\varphi_b = 0.929$. The sign inversion indicates a swelling / deswelling transition. Alike symbols ($\bullet$,$\blacklozenge$) correspond to the same conditions in both a and b parts.

develops in time, but when the LC volume fraction exceeds φ_{NI}, a sign inversion occurs signaling a swelling / deswelling transition process which is described by the growth of $\varphi_a(t)$ in time.

The anisotropy driven deswelling process is further enhanced upon cooling as we see from panel b where we represent τ_0/τ_{sw} vs T^{-1} at $\varphi_b = 0.929$ (corresponding to the symbols in panel a). The isotropic branch starts at $T_C = 347.48$ K $(T_C^{-1} = 0.00288 \text{ K}^{-1})$ and ends at $T = 309.35$ K $(T^{-1} = 0.00323 \text{ K}^{-1})$, where the anisotropic interaction takes over to induce a rapid deswelling of the polymer. The anisotropic branch is constructed from a reproduction of the curves in Figure **9a** at different temperatures. The symbols shown in this branch indicate the conditions at which the calculations were made (see panel a). The swelling / deswelling transition is more pronounced for the LC with higher order such as 8CB, and a cascade of deswelling events takes place as φ_b decreases to reach, first φ_{SN} then φ_{NI}.

Polymerisation Induced Phase Separation (PIPS)

Photo polymerisation induced phase separation is often adopted for the preparation of PDLCs [21, 22], starting from the monomer solution and ending with a solid material dedicated to experimental investigations or practical applications. The time evolution of the mixture from initial to final states experiences a subtle interplay between the kinetics of polymerization, and concomitant phase separation. Understanding, and controlling these combined dynamical processes necessitate a close examination of the phase behaviour, and morphology developments when the polymer size $N_a(t)$, evolves from a single unit to $N_{a\infty}$ monomers per chain. To face this challenging task, let us examine how the phase diagrams of Figures **8a** and **8b** evolve when N_a varies from 1 to 10. Diagrams for different values of N_a were reported before for a variety of systems [23, 24], confirming that both chain length and interactions play major roles in determining the transition lines. The problem to be resolved is to understand how the kinetics and morphology developments, from initial to final states proceed, and how non equilibrium states evolve from the start of polymerization ($t = 0$) through its total implementation, when the final equilibrium state is reached ($t \rightarrow \infty$). We simulate this process starting from the relationship between $N_a(t)$ and the monomer conversion rate $\gamma(t)$, where the latter represents the number of reacted monomers at time t, over the total number of monomers in the initial solution. A model commonly used in the literature suggests the following relationship

$$\gamma(t) = 1 - N_a^{-1}(t). \tag{31}$$

As $t \rightarrow \infty$, $\gamma(t) \rightarrow \gamma_\infty$, which is asymptotically one for a total conversion with no residual monomers. Eq. (31) satisfying the initial conditions, $N_a(t = 0) \approx 1$, and $\gamma(t = 0) \approx 0$, gives access to $N_a(t)$ from the solution of the kinetic equations for $\gamma(t)$. Since $N_a(t)$ varies with time, the system undergoes time developments and, adopting the line of reasoning of reference [13], one finds the following critical parameter $\chi_c(t)$ for isotropic solvents

$$\chi_c^{(i)} = \frac{1}{2\varphi_a N_a(t)} + \frac{1}{2\varphi_b N_b} \tag{32}$$

In the so-called double reaction model, one finds

$$\gamma(t) = \frac{\gamma_0 e^{\kappa t}}{1 + \gamma_0 \left(e^{\kappa t} - 1\right)}, \tag{33}$$

This assumes that, γ_0, the initial conversion ratio is very small but nonzero while at $\kappa t \rightarrow \infty$ (i.e. $\gamma_\infty = 1$) all monomers have reacted, κ being the polymerization reaction rate. The rise of temperature due to the polymerization is ignored assuming that T remains constant below T_{NI}, the order parameter depends only on φ_b and the critical parameter $\chi_c(t)$ is given by

$$\chi_c(t) = \chi_c^{(i)}(t) - \frac{\nu s}{2}\left(s + \varphi_b \frac{\partial s}{\partial \varphi_b}\right) \tag{34}$$

The second term in the right hand side shows that the critical parameter for spinodal decomposition is reduced by the anisotropic interaction. Here, we limited the description to nematic LCs but the reduction of the critical parameter is larger for a higher anisotropy such as in 8CB. Figure **10a** illustrates the changes in the $\chi_c(t)$ vs φ_b curve during polymerisation in the presence of anisotropic solvents. The nematic branch shifts with a broadening in the biphasic region, and the anisotropy speeds up dramatically the phase separation process during the early stages of polymerization. It should be kept in mind that, if the chemical reactions induce a heating above T_{NI}, then the solvent becomes isotropic and the second term in Eq. (34) vanishes, which means that the isotropic part $\chi_c^{(i)}(t)$ alone governs the phase separation process.

According to reference [13], morphology developments during the combined kinetics of polymerization and phase separation are characterized by the following rate of change
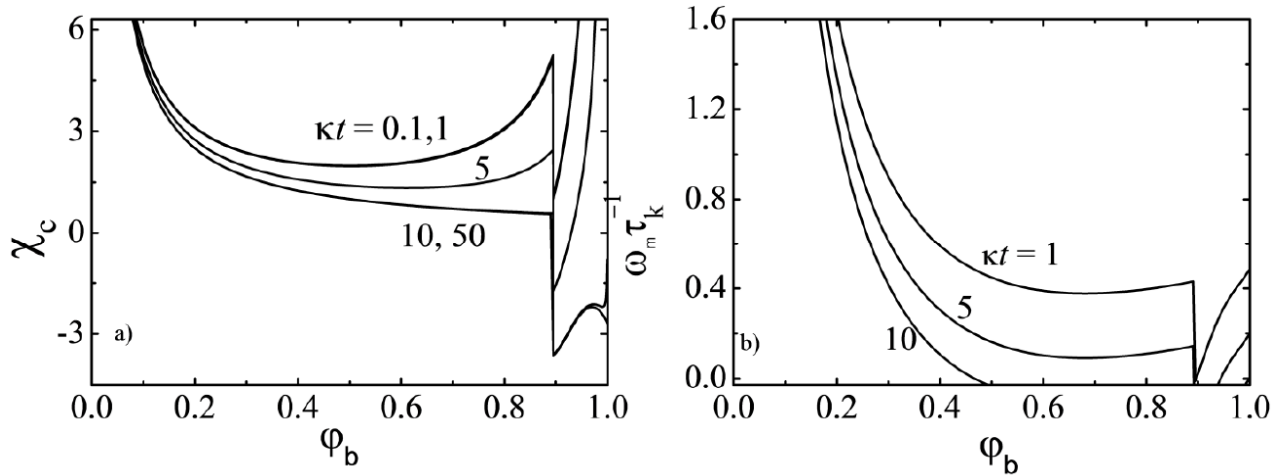
Figure 10: a) $\chi_c(t)$ vs φ_b for a nematic solvent at different times **b)** $\omega_m \tau_k^{-1}$ vs φ_b under similar conditions at $q = 0$ (see Eq. (37)).

$$\tau_k^{-1}(q,t) = 2q^2 k_B T M(q) \left[\chi_c(t) - \chi_{ab}\right]\left[1 + q^2 \xi_c^2(t)\right], \qquad (35)$$

where the mobility $M(q)$ expresses the effects of hydrodynamic coupling modes, and $\xi_c(t)$ designates the range of polymer fluctuations.

$$\xi_c^2(t) = \frac{l^2}{24\phi_a} \frac{1}{\chi_c(t) - \chi_{ab}}. \qquad (36)$$

In the Rouse model, $M(q) = \varphi_a/\zeta$, ($\zeta = 6\pi\eta l$, represents the monomer friction coefficient), and Eq. (35) becomes

$$\left(\omega_m \tau_k\right)^{-1} = \varphi_a \left[\chi_c(t) - \chi_{ab}\right]\left[1 + q^2 \xi_c^2(t)\right];$$
$$\omega_m = q^2 \frac{k_B T}{6\ \eta l} = q^2 D_m, \qquad (37)$$

ω_m is known as the monomer jump frequency. In the presence of the long range hydrodynamic interaction, the generalized mobility $M(q)$ becomes q-dependent and the kinetics are described by a modified characteristic time [13]

$$\tau_{hydro}^{-1} = \omega_m \left(l/\xi_c(t)\right) G\left(q\xi_c(t)\right), \qquad (38)$$

$G(x)$ is the so-called mode coupling function, also referred to as the Kawasaki function, and emerging from the use of the Oseen tensor

$$G(x) = \frac{3}{4} \frac{1+x^2}{x^3} \left\{x + \left(x^2 - 1\right) \arctan x\right\}. \qquad (39)$$

Figure **10b** represents the $(\omega_m \tau_k)^{-1}$ vs φ_b deduced from the $q = 0$ limit of Eq. (38) showing that in the

presence of nematic solvents, anisotropy interactions lead to a drastic slowing down of fluctuations and eventually growth and onset of phase separation. Similar observations may be made in the presence of long range hydrodynamic interaction. Recalling that $G(x = 0) = 1$, one finds in the $q = 0$ limit

$$\tau_{hydro}^{-1} = q^2 \frac{k_B T}{6\pi\eta\xi_c(t)}; \quad \omega_m \tau_{hydro} = l / \xi_c(t). \qquad (40)$$

DISCUSSIONS

The above theoretical formalism was used by Benmouna, Maschke and co-workers [26-30] to analyze the phase behaviour of a variety of systems involving molecular species that differ in nature and architecture. The phase diagrams of the initial monomer solution and the final polymer blend with a variety of LCs such as E7, 5CB and 8CB were reported before considering polymers of different masses, and crosslinked networks.

Despite all the efforts made, PDLCs remain still an active subject of investigation in the literature. We do not intend to present an exhaustive review of this matter, but we are rather inclined to make a biased selection of references, to focus more on how the solvent's anisotropy enhances the phase separation process. The eutectic mixture of LCs, E7, was often used because it is characterized by a relatively high T_{NI} ($\approx$ 333 K), a low crystalline temperature ($\approx$ 243 K), which makes it a good candidate for practical applications. These temperatures favour operating the LC under normal conditions in developing, for example, switchable windows with controlled light transmission. Another commonly used LC is 5CB, which has a

narrower range of operating temperature with $T_{CN} \approx$ 298 K and $T_{NI} \approx 308$ K, while 8CB exhibits smectic-A order and the transition temperatures $T_{SN} \approx 306.5$ K, $T_{NI} \approx 313.5$ K.

With regards to monomers, several species were considered in a variety of experimental studies. Examples are acrylates of different functionalities like the monofunctional n-butyl acrylate [25], the bi functional hexanedioldiacrylate [26] or the trifunctional propoxylated glyceroltriacrylate [27]. Samples involving polystyrene, with different molecular weights [28] ($M_w = 4 \times 10^3$, 2×10^5 g mol^{-1}), poly(dimethylsiloxane) [29], and poly(2-phenoxyethylacrylate) [30] were also investigated.

The effects of molecular weight, composition, crosslinking density for polymer networks, on the phase behaviour and thermophysical properties were analyzed in details using a variety of techniques, and in particular optical microscopy, scanning electron microscopy, differential scanning calorimetry, small angle neutron scattering, and light scattering [31]. These techniques were often combined to obtain the transition from one region of the phase diagram to the other and the data analyzed successfully with formalisms similar to those given here. Only few parameters were adjusted to fit the data. For example, the interaction parameter χ_{ab} was assumed to be function of temperature according to $\chi_{ab} = A + B/T$, and the constants A and B were adjusted to fit the data. Under certain conditions, χ_{ab} was allowed to be function of the polymer concentration as well to improve the fit [32]. Complementary information was obtained from DSC thermograms, and in particular the amount of heat involved in the nematic to isotropic transition ΔH_{NI}, which gives a direct access to the amount of LC remaining in the polymer matrix [33]. This quantity dictates; to a large extend, the performance of PDLC materials, because it changes the index of refraction of the polymer matrix. An important criterion for choosing the polymer in practical applications is based on the matching condition of index of refraction with the ordinary component of the LC in droplets. The LC that remains in the polymer matrix acts as a plasticizer which reduces its mechanical strength, speeds up the aging process, and obviously, it is just a wasted amount of LC.

Polymer brushes, carrying grafted LC groups via spacers with controlled flexibility and length, act as alignment layers, when embedded in a medium containing small LC molecules. Those layers have properties reminiscent of nematogen mixtures, and show a rich phase behaviour which was explored in reference [34]. By considering blends of side chain liquid crystals and small nematic molecules, peculiar phase properties were identified in the diagram, including the tea-pot structure.

PROSPECTS AND CONCLUSIONS

In spite of all the efforts made to understand the properties of nematogens mixtures, there are still many aspects that remain to be elucidated and need further investigations. The choice of polymer with LC behaviour is still a subject of debate concerning both its nature (synthetic or natural) and architecture. Diblock copolymers with a rigid and a flexible part are still a subject of active research, because of their important applications in modern technologies, based on the ordered phases developed from the rigid block. A full characterization of the phase diagram is not yet available at present, and needs further efforts in the future. Multiblock copolymers with a succession of rods and flexible blocks are known as main chain liquid crystal polymers. Their properties can be tuned by changing the number of repeat units according to the needs. A small number of units tend to reproduce the behaviour of a single diblock with a proper modulation, while a multiblock made of a very large number of blocks reproduces essentially the properties of a homopolymer with a renormalized unit. The switching from one type to another and the emergence of new structures and ordered phases need further investigations along the lines of the present work. Side chain LC polymers form a different class of multiblock copolymers whose properties can be tuned by changing the length of the spacer connecting the backbone to the side rod. The assemblies resulting from those multiblocks exhibit a rich variety of structures and phases that are still unexplored. For crosslinked networks made of flexible strands and side chain LC groups, one would expect an entropy driven phase separation with significant consequences of the morphology of PDLCs. The presence of crosslinks, opposing stretching of the strands, modifies the size distribution of droplets where the low molecular weight LCs is confined. Ordering of molecules at the polymer interface is not the same as at the centre of droplets which means that the order parameter has some spatial modulations that should be evaluated in a future work. Polymer brushes carrying side chain LC groups, and acting as alignment layers, represent a variety of options to form the family of nematogen blends, when

embedded in a low molecular weight LC solvent. Not all those systems were studied with sufficient details, and some of them need significant research efforts to explore the fine aspects of their structural properties and phase behaviour. Some biological macromolecules exhibit LC phases under specific conditions and the concepts presented here may help to elucidate certain features of biological functions [35, 36]. We intend to address these questions in the future.

In conclusion, we note that many aspects need to be re-examined, to reach a better understanding of how widely different molecular species, the flexible long chains and the rigid LC molecules, can combine to form a class of materials with dedicated functionalities, and given applications in modern technologies. The present work gives the state of art in some PDLCs properties and suggests possible ways of extension and further developments.

REFERENCES

[1] Singh S, Srivastava JK, Singh, RK. Polymer Dispersed Liquid Crystals. In: Liquid crystalline polymers Springer International Publishing 2016; p. 195-250.
https://doi.org/10.1007/978-3-319-22894-5_7

[2] Yang DK, Wu ST. Liquid crystal materials. In: Fundamentals of liquid crystal devices. John Wiley and Sons, Ltd.: Chichester: UK: 2006: p. 191-212.
https://doi.org/10.1002/0470032030.ch6

[3] Kim Y, Kim K, Kim KB, Park, JY, Lee N, Seo Y. Flexible polymer dispersed liquid crystal film with graphene transparent electrodes. Curr Appl Phys 2016; 16: 409-414.
https://doi.org/10.1016/j.cap.2016.01.003

[4] Liu J, Liu X, Zhen Z. Effects of chiral additives on the electro-optical properties of polymer dispersed liquid crystal. Mater Lett 2016; 163: 142-145.
https://doi.org/10.1016/j.matlet.2015.10.060

[5] Kim M, Park, KJ, Seok S, Ok JM, Jung HT, Choe J, Kim DH. Fabrication of microcapsules for dye-doped polymer-dispersed liquid crystal-based smart windows. Appl Mater Interfaces 2015; 7: 17904-17909.
https://doi.org/10.1021/acsami.5b04496

[6] Torres JC, Vergaz R, Barrios D, Sánchez-Pena JM, Viñuales A, Grande HJ, Cabañero G. Frequency and temperature dependence of fabrication parameters in polymer dispersed liquid crystal devices. Materials 2014; 7: 3512-3521.
https://doi.org/10.3390/ma7053512

[7] Srivastava JK, Singh RK, Dhar R, Singh S. Thermal and morphological studies of liquid crystalline materials dispersed in a polymer matrix. Liq Cryst 2011; 38: 849-859.
https://doi.org/10.1080/02678292.2011.583995

[8] Perju E, Paslaru E, Marin L. Polymer-dispersed liquid crystal composites for bio-applications: thermotropic, surface and optical properties. Liq Cryst 2015; 42: 370-382.
https://doi.org/10.1080/02678292.2014.992055

[9] Kumar P, Sharma V, Jaggi C, Raina KK. Dye-dependent studies on droplet pattern and electro-optic behaviour of polymer dispersed liquid crystal. Liq Cryst 2016; 1-11.
https://doi.org/10.1080/02678292.2016.1247476

[10] Kawata Y, Yamamoto T, Kihara H, Yamamura Y, Saito K, Ohno K. Three gel states of colloidal composites consisting of polymer-brush-afforded silica particles and a nematic liquid

[11] Kularatne RS, Kim H, Boothby JM, Ware, TH. Liquid crystal elastomer actuators: Synthesis, alignment, and applications. J Macromol Sci B 2017; 55, 395-411.
https://doi.org/10.1002/polb.24287

[12] Kyu T, Chiu HW. Morphology development during polymerization-induced phase separation in a polymer dispersed liquid crystal. Polymer 2001; 42: 9173-9185.
https://doi.org/10.1016/S0032-3861(01)00389-5

[13] Benmouna F, Bouabdellah-Dembahri Z, Benmouna M. Polymerization-induced phase separation: phase behavior developments and hydrodynamic interaction. J Macromol Sci B 2013; 52: 998-1008.
https://doi.org/10.1080/00222348.2012.748617

[14] Deshmukh RR. Electro-optic and Dielectric Responses. In: PDLC composite systems. In: Liquid crystalline polymers. Springer International Publishing 2015; p. 169-195.
https://doi.org/10.1007/978-3-319-20270-9_7

[15] Wermter H, Finkelmann H. Liquid crystalline elastomers as artificial muscles. e-Polymers 2001; 1: 111-123.
https://doi.org/10.1515/epoly.2001.1.1.111

[16] Benmouna F, Maschke U, Coqueret X, Benmouna M. Theoretical phase behavior of crosslinked polymers and liquid crystals. Macromol Theory Simul 2001; 10: 63-70.
https://doi.org/10.1002/1521-3919(20010101)10:1<63::AID-MATS63>3.0.CO;2-P

[17] Benmouna F, Maschke U, Coqueret X, Benmouna M. Miscibility in cross-linked polymer-solvent systems with nematic interactions. Macromolecules 2000; 33: 1054-1062.
https://doi.org/10.1021/ma990517z

[18] Benmouna F, Maschke U, Coqueret X, Benmouna M. Equilibrium phase behavior of polymer and liquid crystal blends. Macromol Theory Simul 2000; 9: 215-229.
https://doi.org/10.1002/1521-3919(20000601)9:5<215::AID-MATS215>3.0.CO;2-R

[19] Benmouna F, Coqueret, X, Maschke U, Benmouna M. Phase behavior of blends of polymers and smectic-A liquid crystals. Macromolecules 1998; 31: 4879-4890.
https://doi.org/10.1021/ma9804038

[20] Benmouna F, Maschke U, Coqueret X, Benmouna M. Effects of nematic coupling on the phase behaviour of nematogen mixtures. Polym Int 2001; 50: 469-474.
https://doi.org/10.1002/pi.659

[21] Park S, Kim HK, Hong JW. Investigation of the photopolymerization-induced phase separation process in polymer dispersed liquid crystal. Polym Test 2010; 29: 886-893.
https://doi.org/10.1016/j.polymertesting.2010.05.015

[22] Nwabunma D, Chiu HW, Kyu T. Theoretical investigation on dynamics of photopolymerization-induced phase separation and morphology development in nematic liquid crystal/polymer mixtures. J Chem Phys 2000; 113: 6429–6436.
https://doi.org/10.1063/1.1309537

[23] Benmouna F, Maschke U, Coqueret X, Benmouna M. Miscibility in cross-linked polymer-solvent systems with nematic interactions. Macromolecules 2000; 33: 1054-1062.
https://doi.org/10.1021/ma990517z

[24] Benmouna F, Maschke U, Leclercq L, Ewen B, Coqueret X, Benmouna M. On the miscibility of crosslinked networks and solvents with and without nematic order. Mol Cryst Liq Cryst A 1999; 330: 1709-1717.
https://doi.org/10.1080/10587259908025623

[25] Bouchaour T, Benmouna F, Leclercq L, Ewen B, Coqueret X, Benmouna M, Maschke U. Phase equilibrium of poly(n-butyl acrylate) and E7. Liq Cryst 2000; 3: 413-420.
https://doi.org/10.1080/026782900202877

[26]   Roussel F, Maschke U, Buisine JM, Coqueret X, Benmouna F. Phase properties of hexanedioldiacrylate/E7 blends. Mol Cryst Liq Cryst 2001; 365: 1641-1649.
https://doi.org/10.1080/10587250108025347

[27]   Maschke U, Benmouna F, Roussel F, Daoudi A, Gyselinck F, Buisine JM, Coqueret X, Benmouna, M. Phase diagrams of cured and uncured propoxylated glyceroltriacrylate/5CB mixtures. Macromol Chem Phys 2001; 202: 1100-1104.
https://doi.org/10.1002/1521-3935(20010401)202:7<1100::AID-MACP1100>3.0.CO;2-I

[28]   Benmouna F, Daoudi, A, Roussel F, Leclercq L, Buisine JM, Coqueret X, Benmouna M, Ewen B, Maschke U. Effect of molecular weight on the phase diagram and thermal properties of poly(styrene)/8CB mixtures. Macromolecules 2000; 33: 960-967.
https://doi.org/10.1021/ma991228d

[29]   Gogibus N, Maschke U, Benmouna F, Ewen B, Coqueret X, Benmouna M. Phase diagrams of poly(dimethylsiloxane) and 5CB blends. J. Polym. Sci Part B: Polym Phys 2001; 5: 581-588.
https://doi.org/10.1002/1099-0488(20010301)39:5<581::AID-POLB1031>3.0.CO;2-Z

[30]   Bouchaour T, Benmouna F, Roussel F, Buisine JM, Coqueret X, Benmouna M, Maschke U. Equilibrium phase diagram of poly(2-phenoxyethylacrylate) and 5CB. Polymer 2001; 4: 1663-1667.
https://doi.org/10.1016/S0032-3861(00)00403-1

[31]   Benmouna F, Peng B, Gapinski J, Patkowski A, Ruhe J, Johannsmann D. Dynamic light scattering from liquid crystal polymer brushes swollen in a nematic solvent. Liq Cryst 2001; 28: 1353-1360.
https://doi.org/10.1080/02678290110061395

[32]   Benmouna F, Maschke U, Coqueret X, Benmouna M. On the phase equilibria of nematic mixtures. J Polym Sci Part B: Polym Phys 2000; 38: 478-485.
https://doi.org/10.1002/(SICI)1099-0488(20000201)38:3<478::AID-POLB13>3.0.CO;2-Q

[33]   Maschke U, Benmouna F, Roussel F, Daoudi A, Gyselinck F, Buisine JM, Coqueret X, Benmouna M. Phase diagrams of cured and uncured propoxylated glyceroltriacrylate/5CB mixtures. Macromol Chem Phys 2001; 202: 1100-1104.
https://doi.org/10.1002/1521-3935(20010401)202:7<1100::AID-MACP1100>3.0.CO;2-I

[34]   Benmouna F, Peng B, Ruhe J, Johannsmann D. Phase diagrams of phenyl benzoate side group liquid crystal polymers and similar low molecular mass liquid crystals. Liq Cryst 1999; 26: 1655-1661.
https://doi.org/10.1080/02678292.1999.11509449

[35]   Khan M, Park SY. Liquid crystal-based biosensor with backscattering interferometry: A quantitative approach. Biosensors and Bioelectronics 2017; 87: 976-983.
https://doi.org/10.1016/j.bios.2016.09.065

[36]   Khosla S, Lal S, Sood N, Bawa SS, Singh N. Liquid crystal elastomers in biological applications: a review. Int J Theor Appl Sci 2011; 3: 67-75.